Inter/Intramolecular Cerenkov Radiation Energy Transfer (CRET) from a fluorophore with a built-in radionuclide.

Supporting Information

Yann Bernhard,[‡] Bertrand Collin,[‡,§] Richard Decréau[‡]*

[‡] University of Burgundy, Chemistry Department, ICMUB Institute, 21078 Dijon (France)

[§] Comprehensive Cancer Center George-François Leclerc (CGFL), Nuclear Medicine Department, Preclinical Imaging Platform, 21079 Dijon (France)

Richard.Decreau@u-bourgogne.fr

Outline:

1. Materials and Methods

1.1. Chemicals and Radionuclides

→ ***Chemicals*** used in this study are from various providers: Acros Organics [5-aminofluorescein (pure, ref. 400770050), fluorescein (99 %, ref. 410620010), rhodamine 6G (99 %, ref. 419025000), rhodamine 101 inner salt (99 %, ref. 419060010), *N,N*-dimethylformamide extra dry (99.8 %, ref. 348431000)]; Chematech [2,2',2''-(10-(2,6-dioxotetrahydro-2H-pyran-3-yl)-1,4,7,10-tetraazacyclododecane-1,4,7-triyl)triacetic acid (C109)]; Strem Chemicals [yttrium chloride hexahydrate (99.9 %, ref. 93-3903)]. All chemicals and solvents were used as supplied without further purification.
→ ***Radionuclides*** are from the following providers: [^{18}F]-FDG (Glucotep®) is from Cyclopharma (France); [^{177}Lu]-$LuCl_3$ and [^{90}Y]-YCl_3 are from Perkin-Elmer (USA).

1.2. Purification methods

Compounds **1** was purified on flash column chromatography equipped with a C18 column using CH_3CN/ 0.1 % HCOOH; H_2O/ 0.1 % HCOOH as the eluent.
Compound **^{89}Y-1** was purified using a Dionex Ultimate 3000 semi-preparative column chromatography equipped with a C18 column. The method employed was the following: eluent A: CH_3CN/ 0.1 % TFA; eluent B: H_2O/ 0.1 % TFA; flow: 2.8 mL/min; ramp from A/B 10:90 to 50:50 in 40 min then A/B 50:50 during 5 min; return in 1 min to initial conditions; detector: 200 nm, 300 nm, 500 nm.

1.3. Characterizations

1.3.1. NMR spectroscopy

Measurements were performed on a Bruker Dalton X, at 600 MHz (^{1}H) and at different temperature (from 300 to 420 K) to resolve the signals of the macrocyclic moities. Samples were analyzed in anhydrous deuterated DMSO or deuterated water containing a little amount of deuterated sodium hydroxide solution (*ca.* 5-10 mg/600 µL DMSO-d_6 or D_2O/NaOD mixture). Chemical shifts reported as δ in ppm relative to TMS (residual DMSO from deuterated DMSO chemical shift was set at 2.50 ppm and residual water from deuterated D_2O at 4.79 ppm) and coupling constants expressed in Hz. The following abbreviations were used to describe the spin multiplicity: s= singlet, d= doublet, t= triplet, m= multiplet.

1.3.2. MALDI-TOF MS (Matrix-Assisted Laser Desorption/Ionisation - Time of Flight Mass Spectroscopy)

Measurements were performed on a Ultraflex II LRF 2000 apparatus (BRUKER), using 2,5-hydroxybenzoic acid (DHB) as a matrix. Solutions were prepared upon dissolving 1 mg of compound into 1 mL of water.

1.3.3. ESI-Q MS (ElectroSpray Ionisation-Quadripole Mass Spectroscopy)

Measurements were performed on a LTQ Orbitrap XL (THERMO) coupled to HPLC Ultimate 3000 (DIONEX). 1 mg of compound was dissolved into 1 mL of appropriate solvent then diluted 100 times with methanol.

1.3.4. UV-Visible spectroscopy

Spectra were performed on a Shimadzu UV-2550 spectrophotometer using glass cuvettes 1x1x3 cm (1 cm path).

1.3.5. HPLC (High Performance Liquid Chromatography)

Compounds were analyzed on a Dionex Ultimate 3000 apparatus, equipped with a Chromolith High Resolution RP-18 column (5-4.6 mm, Merck). The Method used was the following: eluent A: CH_3CN + 0.1 % TFA; eluent B: H_2O + 0.1 % TFA; flow: 3 mL/min; equilibrate for 1 min 45 min afterwards; ramp from 100 % B to 100 % A; duration: 5 min; keep constant for 1 min; return in 1.5 min to initial conditions; detector: 214 nm, 230 nm, 254 nm, 500 nm.

1.3.6. Radiolabelling validation: Radio-TLC

The radiolabelled compound **^{90}Y-1** was deposited on silica gel TLC plates (at 1 cm height), and eluted with methanol / 1 M ammonium acetate buffer mixture (1:1 vol.) (until 5 cm height). Radioactivity was detected using an AR-2000 radio-TLC scanner (Bioscan, USA).

1.3.7. Fluorescence measurement

→ *Non-Radioactive* Fluorescence measurements (for **1** and **^{89}Y-1**) were performed on a Jasco FP-8500 spectrofluorometer equipped with a Xe source. Fluorescence quantum yields were calculated using fluorescein in NaOH 0.1 M as reference (Φ_F= 0.91). Excitation was performed at 470 nm for both sample and reference. Emission spectra were recorded for an absorbance at excitation wavelength (470 nm) in the range of 0.03 to 0.07. Fluorescence quantum yields (Φ_F) were determined by the comparison method, using the following equation:

$$\phi_F = \phi_F(Std) \times \left(\frac{\eta}{\eta(Std)}\right)^2 \times \left(\frac{1-10^{-Abs}}{1-10^{-Abs(Std)}}\right) \times \left(\frac{A(Std)}{A}\right) \qquad (Eq\ 1)$$

With:
Std corresponds to standard (Fluorescein)
Φ_F and Φ_F(Std): fluorescence quantum yields
η and η(Std): refractive index of the solvent

Abs and Abs(Std): absorbances at excitation wavelength
A and A(Std): areas under the fluorescence curves

→ *Radioactive* Cerenkov Radiation Energy Transfer (CRET) Fluorescence measurements were performed on a Agilent Cary Eclipse (sensitivity: *a)* signal-to-noise measurements of Raman band of water 1/700; *b)* theoretical detection limit: 1 pmol of fluorescein) in quartz cuvettes 1x1x3 cm (1 cm path). The method used was the following: 400 µL of fluorophore (10^{-3} M, 5×10^{-4} M, 10^{-4} M in a water-miscible solvent) was mixed with a solution of the radioactive species (i.e. [^{18}F]-FDG, [^{177}Lu]-$LuCl_3$ and [^{90}Y]-YCl_3), the volume of which was varied because it depended upon the desired level of radioactivity to introduce in the cuvette. Subsequent addition of a saline solution (0.9% NaCl) was achieved to reach an overall volume of 1 mL. Measurement parameters were: bioluminescence mode, gate time of 10 s, 20 nm emission slit, 3 nm of data interval, Stavinsky smoothing (factor 5).

1.3.8. Nuclear Safety

Safety Rules were set at the George-François Leclerc Research Center (CGFL) preclinical Imaging platform. They comply with the standards of the French Nuclear Safety Agency (ASN). Radioactivity was measured with a dose calibrator (MEDI 405, Medisystem, France).

2. Luminescence Studies

2.1. Curve interpretation

Baseline curves were found to be pretty dependent upon the volume of saline solution added and the nature of the solvent in the fluorophore solution. That is why, to be comparable, curves were adjusted to a same value at 700 nm by subtraction with an adapted constant value.

2.2. Cerenkov Photons

Mitchell's simulations (Mitchell, G. S. *et al. Phil. Trans. R. Soc. A* **2011**, *369*, 4605) gave an estimate of the number of photons emitted per radioactive decay (^{90}Y: 70 photons; ^{18}F: 1.3 photons), it is possible to get a rough estimate of the overall number of photons emitted from a given number of radionuclides *n* available. Note that Mitchell's calculation relied on the formula established by Franck-Tamm (Franck, I. M.; Tamm, I. E.; *Dokl Akad Naukl SSSR*, **1937**, *14*, 109-114) and Jelley (Jelley, J. V. *Cerenkov Radiation and its applications* (London, Pergamon) 1958) and later by Levin and Hoffman (Levin, C. S. Hoffman, E. J. *Phys Med. Biol.* **1999**, 44, 781-99) and Spinelli and Boschi (Spinelli, A. E.; et al. *Phys Med. Biol.* **2010**, *55*, 483-495).

2.3. CRET Ratios / quantum efficiency

→ CRET quantum efficiency was calculated using the method developed for FRET and BRET (see: a) Jares-Erijman, E. A.; Jouin, T. M.; *Nat. Biotechnol.***2003**, *21*, 1387-1395; b) Gammon, S.; Villalobos, V; Roshal, M.; Samrakandi, M.; Piwnica-Worms, D., *Biotechnol. Prog.* **2009**, *25*, 559-569; c) Xu, Y.; Piston, D. W.; Johnson, C. H. *Proc.*

Natls.Acad. Sci. U. S. A. **1999**, *96*, 151-156.) and adapted by Piwnica-Worms (Dothager, R. S.; Goiffon, R. J.; Jackson, E.; Harpstrite, S.; Piwnica-Worms, D. *PLoS ONE*, **2010**, *5*, e13300) as follows.

Piwnica-Worms's formula calculated CRET as "the quotient of light detected within a spectral window (X) centered on the fluorophore emission divided by light detected within a spectral window (Y) of the Cerenkov Radiation emission, **minus** the quotient of light detected in windows X and Y in the presence of CR alone.

$$CRET\ (X) = \frac{CR+Fluorophore\ (X)}{CR+Fluorophore\ (Y)} - \frac{CR(X)}{CR(Y)} \qquad (Eq\ 3)$$

With:
Spectral window (X): defined as 475-600 nm for Fluoresceine (below), 525-650 nm for Rhodamine 6G and 580-700 nm for Rhodamine 101.
Spectral window (Y): total spectral window (400-700 nm) minus spectral window (X). (Fig. S1.)

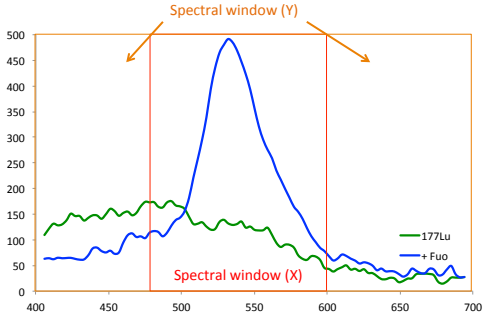

Fig. S1. Spectral windows (X) and (Y) defined for ^{177}Lu (193 MBq) and fluorescein (0.4 µM).

2.4. Results

2.4.1. Cerenkov Radiation (CR) [^{18}F]-FDG

Note that the CR maximum emission is within 350 and 700 nm, with maximum luminescence intensity at 495 nm.

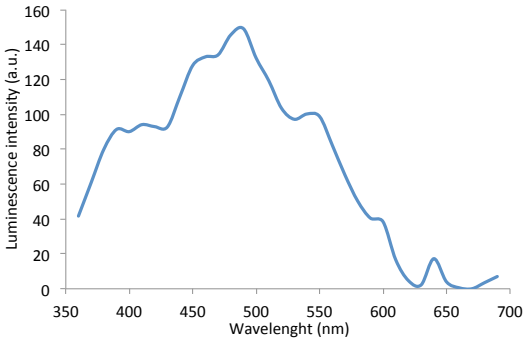

Fig. S2. Emission spectrum of [^{18}F]-FDG (50 MBq) from 350 to 700 nm.

2.4.2. CR/Energy: Fluorescein, Rhodamine / ^{18}F, ^{177}Lu, ^{90}Y

	Fluorescein	Rhodamine 6G	Rhodamine 101
Structure	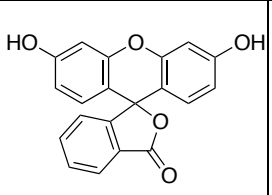	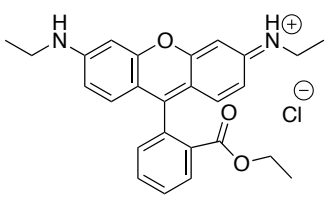	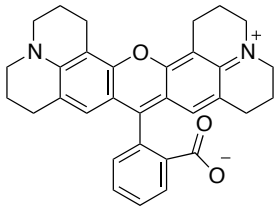
Solvent	NaOH 0.1 M	MeOH	MeOH
Absorbtion maximum wavelength (nm)	490	530	576
Emission maximum wavelength (nm)	514	552	600
Fluorescence quantum yield	0.95	0.94	1
Molar extinction coefficient ($\times 10^{-3}$ mol.cm^{-1})	77	116	95
Brightness ($\times 10^{-3}$ mol.cm^{-1})	73	109	95

Table S1: Optical Properties of the Fluorophores.

A. [^{18}F]-FDG, 53-61 MBq

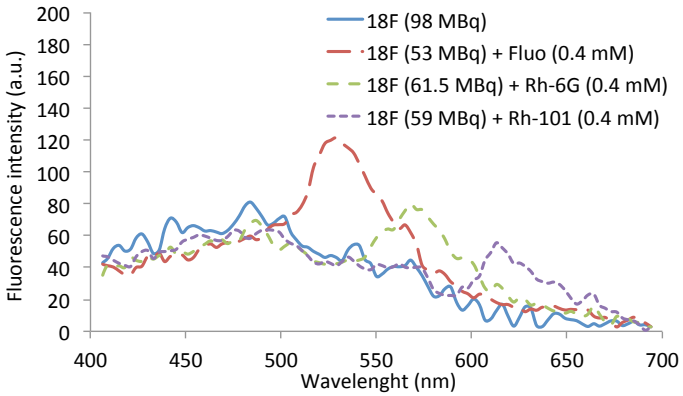

B. [^{177}Lu]-$LuCl_3$: 180-193 MBq (as shown in Fig. 2B)

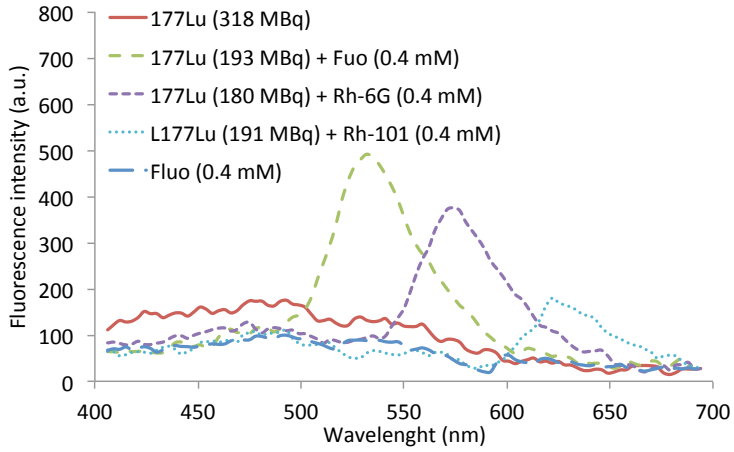

C. [^{90}Y]-YCl_3 : 9.45-9.73 MBq

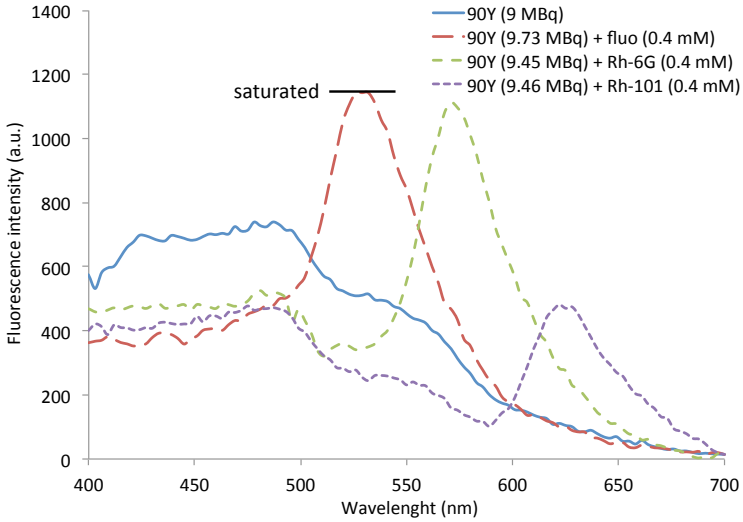

Fig. S3. Excitation of Fluorescein, Rhodamine 6G, and Rhodamine 101 with [^{18}F]-FDG (ca. 50 MBq, spectrum A), [^{177}Lu]-$LuCl_3$ (ca 185 MBq, spectrum B) and [^{90}Y]-YCl_3 (ca. 9.5 MBq, spectrum C).

Comments: Note that because ^{90}Y is a strong emitter (β^-, 2280 keV), lower amounts of radioactivity were required. Also, the emissions max measured were the followings:
Fluorescein: λ_{em}= 532 nm (instead of 514 nm)
Rhodamine 6G: λ_{em}= 574 nm (instead of 552 nm)
Rhodamine 101: λ_{em}= 622 nm (instead of 600 nm)
This 20 nm red-shift is probably because of the high concentrations used that may induce some stacking, which subsequently affects the optical properties of the fluorescent probe.

	Radionuclide	Fluorescein	Rhodamine 6G	Rhodamine 101
A	**^{18}F** (50-60 MBq)	0.82	0.41	0.24
B	**^{177}Lu** (180-190 MBq)	2.09	0.95	0.63
C	**^{90}Y** (9-9.5 MBq)	1.65	0.78	0.32

Table S2. Calculation of CRET ratios between Fluorescein, Rhodamine 6G, Rhodamine 101 and [^{18}F]-FDG, [^{177}Lu]-$LuCl_3$, [^{90}Y]-YCl_3.

The CRET Ratio were compared for a given fluorophore and a series of radionuclides, and for given radionuclide and a series of fluorophores. Altogether, the combination of these results shows that the transfer efficiency is a function of the fluorophore absorption wavelength.

2.4.3. CRET / Titration of Radionuclide and Fluorophore

A. Titration ^{177}Lu activity + fluorescein 0.4 mM:

A progressive increase of activity leads to a linear increase of fluorescence measured at 532 nm. To conclude, the number of emitted photons is directly proportional to the engaged activity. The *detection limit* is around 50 MBq of ^{177}Lu, which corresponds to 1 mBq of ^{90}Y (at 0.4 mM fluorescein).

A.

^{177}Lu activity	CRET ratio
44	0.43
73	0.76
127.5	1.28
170.6	1.63
193	2.09

B.

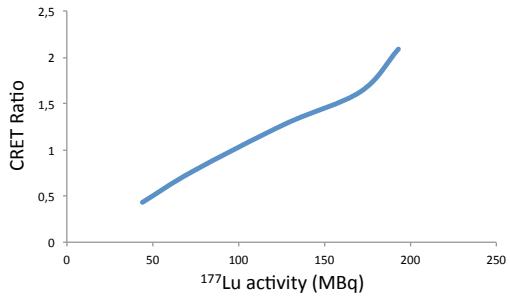

Table S3. Calculation of CRET ratios between fluorescein and ^{177}Lu for different ^{177}Lu activity (A) and CRET Ratio as a function of ^{177}Lu activity (B).

B. Titration fluorescein concentration + ^{90}Y 9-10 MBq:

Comments: Note that the emission max measured changes with dilution. At high concentrations, emission is 20 nm red-shifted compared to values obtained at low concentrations. This phenomenon may be due to stacking, which strongly affects optical properties. However, emission maxima obtained at low concentrations (ca. µM) concur with values reported in the literature.
Moreover, the CRET ratio as a function of fluorescein concentration (Table S4. B.) is not linear probably, most likely because of this *stacking* issue.

A.

Fluorescein Conc.	CRET ratio
0.004	0.46
0.04	0.85
0.02	1.0
0.4	1.76
0.2	1.85

B.

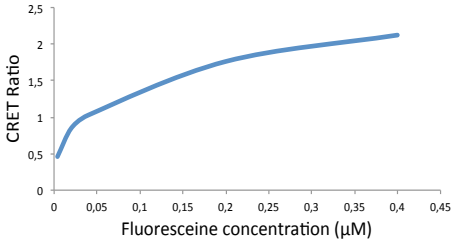

Table S4. Calculation of CRET ratios between fluorescein and [^{90}Y]-Yttrium for different concentrations of fluorescein (A) and CRET ratio as a function of fluorescein concentration (B).

2.4.4. Other fluorophores (Edge-of-CR-absorbing (near-IR-like) fluorophores)

Several other fluorophores have been examined, in the presence of high activities of emitters. CRET was only observed for tetrasulfonated tetraphenylporphyrin (TPPS) in the presence of ^{90}Y (Fig. S4).

Fluorophores:

- Rhodamine B (MeOH, λ_{ex}= 490 nm, λ_{em}= 514 nm, Φ_F= 91-95 %)
- Quinine sulfate (in H_2SO_4 0.5 M, λ_{ex}= 347 nm, λ_{em}= 448 nm, Φ_F= 55 %)
- TPPS (MeOH, λ_{ex}= nm, λ_{em}= 675 nm, Φ_F= %)
- Indocyanine green (MeOH, λ_{ex}= 805 nm, λ_{em}= 835 nm, Φ_F= 11 %)

Radionuclide	Fluorophore	Solvent	Activity (MBq)	Fluorescence
^{18}F	Rhodamine B	MeOH	45-63	None
	Quinine sulfate	EtOH	45	None
	TPPS	Buffer (pH 8)	45	None
^{177}Lu	TPPS	Buffer (pH 8)	192	None
^{90}Y	TPPS	Buffer (pH 8)	9	660 nm
	Indocyanine green	H_2O	18	None

Table S5. Fluorophores examined for CRET (with a Carry-Eclipse Agilent apparatus).

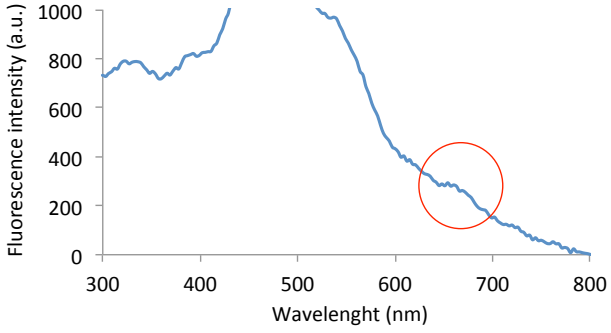

Fig. S4. CRET and fluorescence emission from porphyrin TPPS (^{90}Y, 9 MBq).

2.4.5. 1 and ^{89}Y-1 syntheses (non radioactive)

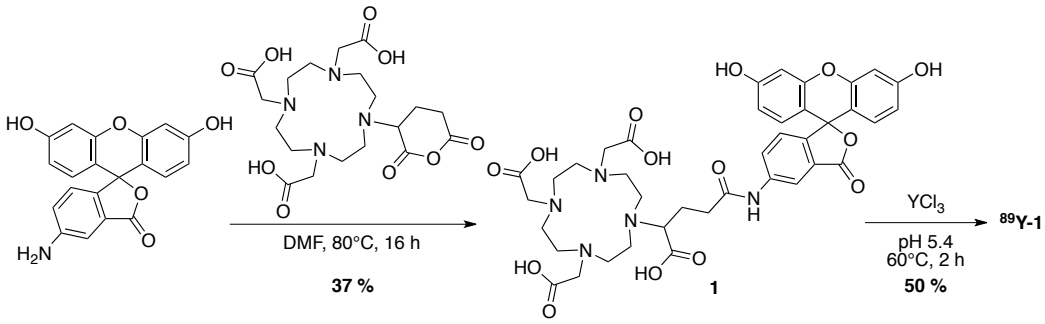

Fig. S5. Synthetic Scheme for the syntheses of **1** and **^{89}Y-1**.

Protocols are described in section 3.1.1 and 3.1.2.

2.4.6. ^{89}Y-1 photophysical properties (non radioactive)

Absorption and fluorescence properties of fluorescein derivatives are highly pH-dependent. We determined that, as for free fluorescein, the maximum quantum yield and the molar extinction coefficient are obtained for a pH equal or higher than 8 (Fig S4-S5). Depending on the pH it is well known that two forms coexist: one is strongly fluorescent, whereas the other one is poorly fluorescent (see below).

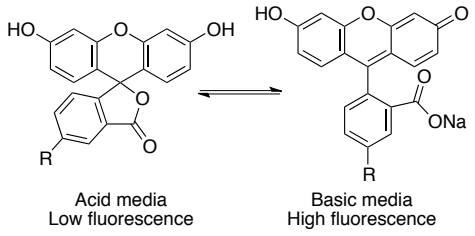

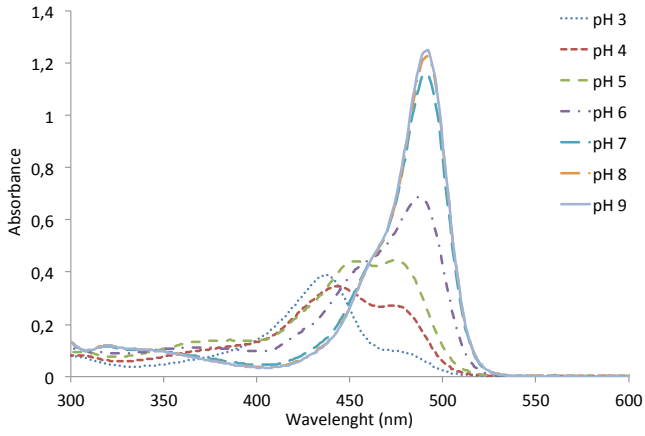

Fig. S6. Absorbtion spectrum of **^{89}Y-1** at various pH values.

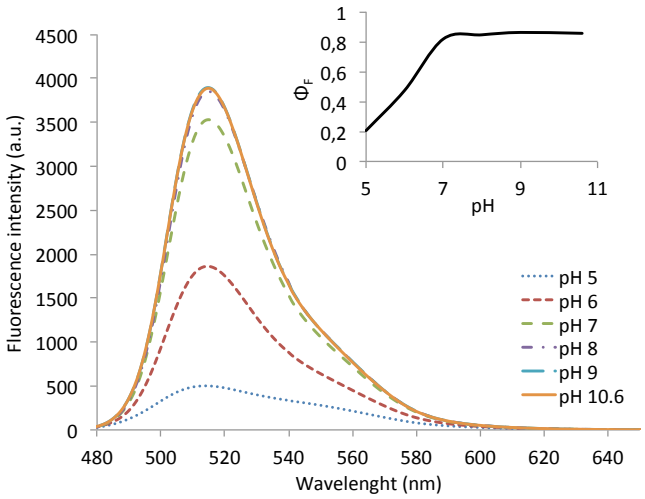

Fig. S7. Emission spectrum of **^{89}Y-1** at various pH values. Insert: fluorescence quantum yield is a function of pH.

2.4.7. ^{90}Y-1. Ratio between ^{90}Y and fluorescein (radiolabelled)

→ The amount of radioactive substance (such as ^{90}Y, ^{177}Y, ^{18}F) was obtained from the following equation:

$$n = \frac{A \times t_{1/2}}{N_A \times \ln(2)} \qquad (Eq\ 2)$$

With:
A: activity (Bq)
n: amount of substance (mol)
$t_{1/2}$: half-life time (s)
N_A: Avogadro constant (mol^{-1})

→ The molar ratio between the amount of radioactive substance ($n(^{90}Y)$) and the amount of fluorescence probe ($n(\mathbf{1})$) could be obtained as follows:

	Volume of **1** solution (µL)[a]	$n(\mathbf{1})$ (mol)	Activity (MBq)	$n(^{90}Y)$ (mol) [b]	Molar ratio[c]
Experiment 1	100	4×10^{-5}	8.953	4.942×10^{-12}	8.1×10^{6}
Experiment 2	50	2×10^{-5}	7.975	4.402×10^{-12}	2.2×10^{6}
Experiment 3	10	4×10^{-6}	8.018	4.426×10^{-12}	9.0×10^{5}
Experiment 4	5	2×10^{-6}	8.743	4.826×10^{-12}	4.4×10^{5}

[a]See section 3.1.3 below
[b]Calculated as with *Eq 2*
[c]Obtained as follow: $\frac{n(\mathbf{1})}{n(90Y)}$ (*Eq 4*)

Table S6. Calculation of molar ratio between **1** and **^{90}Y.**

To conclude, in experiments 1-4 there are 8,100,000; 2,200,000; 900,000; and 440,000 mol of **1** per mol of ^{90}Y, respectively.

2.4.8. Titration ^{90}Y-1 concentration.

A.

Conc of ^{90}Y-1 (mM)	CRET ratio
0.02	0.88
0.04	0.92
0.2	1.27
0.4	1.85

B.

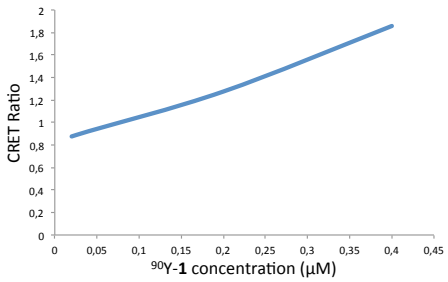

Table S7. A. Calculation of CRET ratios for different concentrations of **^{90}Y-1** (at a constant activity). B. CRET Ratio as a function of fluorescein concentration.

3. Syntheses and Radiolabelling

3.1.1. Fluorescein-DOTA 1

2,2',2''-(10-(1-carboxy-4-((3',6'-dihydroxy-3-oxo-3*H*-spiro[isobenzofuran-1,9'-xanthen]-5-yl)amino)-4-oxobutyl)-1,4,7,10-tetraazacyclododecane-1,4,7-triyl)triacetic acid (**1**). A mixture of 5-aminofluorescein (100 mg, 0.29 mmol) and DOTAGA-anhydride (264 mg, 0.48 mmol) was stirred in DMF (3 mL) under nitrogen atmosphere, at 80°C during 16 hours. The solvent was evaporated off under reduced pressure. The residual solid was taken in acetone (10 mL), filtered off, washed with acetone (3 × 10 mL), and dried under reduced pressure. The yellow solid obtained was diluted in a water/acetonitrile mixture (70:30 vol., 5 mL), and purified by reverse phase column chromatography (C18, 100 % water during 10 min then 30 min ramp until H_2O/CH_3CN 60:40 vol.) to afford compound **1** (85 mg, 37 %).

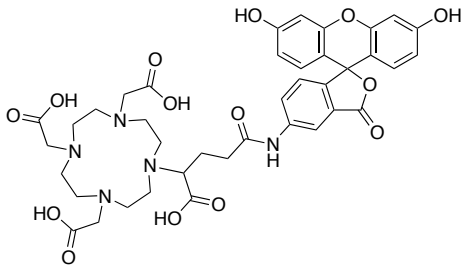

^{1}H NMR (600 MHz, DMSO-d_6, 420 K): δ (ppm)= 1.97 (m, 1H); 2.11 (m, 1H); 2.71 (m, 2H); 2.80 (m, 2H); 3.00 (m, 14H); 3.44 (m, 6H), 3.50 (s, 1H); 6.56 (dd, ^{3}J= 8.6 Hz, ^{4}J= 2.3 Hz, 2H); 6.61 (dd, ^{3}J= 8.6 Hz, ^{4}J= 1.6 Hz, 2H); 6.68 (d, ^{4}J= 2.3 Hz, 2H); 7.08 (d, ^{3}J= 8.3 Hz, 1H); 8.07 (d, ^{3}J= 8.3 Hz, 1H); 8.39 (d, ^{4}J= 1.5 Hz, 1H), 10.75 (s, 1H). MALDI-TOF: m/z= 806.134 $[M+H]^+$ (calcd for $C_{39}H_{44}N_5O_{14}^+$: 806.29), 828.128 $[M+Na]^+$ (calcd for $C_{39}H_{43}N_5O_{14}Na^+$: 828.27), 844.103 $[M+K]^+$ (calcd for $C_{39}H_{43}N_5O_{14}K^+$: 844.24), 850.112 $[M-H+2Na]^+$ (calcd for $C_{39}H_{42}N_5O_{14}Na_2^+$: 850.25), 866.090 $[M-H+Na+K]^+$ (calcd for $C_{39}H_{42}N_5O_{14}KNa^+$: 866.23), 882.069 $[M-H+2K]^+$ (calcd for $C_{39}H_{42}N_5O_{14}K_2^+$: 882.20). HR-MS ESI: m/z= 806.28669 $[M+H]^+$ (calcd for $C_{39}H_{44}N_5O_{14}^+$: 806.28793), 828.26746 $[M+Na]^+$ (calcd for $C_{39}H_{43}N_5O_{14}Na^+$: 828.26987). UV-Vis (NaOH 0.1 M in water), λ_{max} (nm) (ε × 10^3 L.mol^{-1}.cm^{-1}): 491 (76.0). Fluorescence (NaOH 0.1 M in water), λ_{max} (nm) (Φ_F): 515 (0.702).

3.1.2. Fluorescein-DOTA ^{89}Y-1 (non-radiolabelled)

2,2',2''-(10-(1-carboxy-4-((3',6'-dihydroxy-3-oxo-3*H*-spiro[isobenzofuran-1,9'-xanthen]-5-yl)amino)-4-oxobutyl)-1,4,7,10-tetraazacyclododecane-1,4,7-triyl)triacetic acid yttrium complex (**^{89}Y-1**). A solution of **1** (20 mg, 0.025 mmol) in water (5 mL) was adjusted to pH 7 using 1M sodium hydroxide solution. A solution of yttrium chloride (8.3 mg, 0.027 mmol) in 1 mL of water was added under agitation. The mixture was heated at 60 °C during 1 hour. The water in the reaction mixture was evaporated off under reduce pressure. The residual solid was taken in acetone (10 mL), filtered off, washed with acetone (3 × 10 mL) and dried under reduced pressure. The yellow solid obtained was diluted in a water/acetonitrile mixture (50:50 vol., 5 mL) and purified by semi-preparative reverse phase column chromatography (C18, CH_3CN/H_2O 10:90 to 50:50 vol. in 40 min) to afford compound **^{89}Y-1** (11 mg, 50 %).

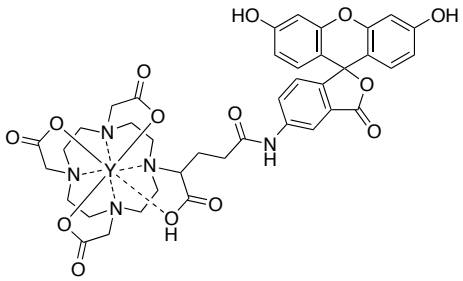

^{1}H NMR (600 MHz, DMSO-d_6, 390 K): δ (ppm)= 1.97 (m, 2H); 2.65-3.18 (m, 18H); 3.49-3.63 (m, 6H); 3.75 (s, 1H); 6.56 (dd, ^{3}J= 8.6 Hz, ^{4}J= 2.4 Hz, 2H); 6.61 (dd, ^{3}J= 8.6 Hz, ^{4}J= 3.5 Hz, 2H); 6.68 (d, ^{4}J= 2.4 Hz, 1H); 7.12 (d, ^{3}J= 8.3 Hz, 1H); 7.86 (dd, ^{3}J= 8.3 Hz, ^{3}J= 1.9 Hz, 1H); 8.25 (d, ^{4}J= 1.9 Hz, 1H), 10.13 (s, 1H). MS MALDI-TOF: m/z= 892.121 $[M+H]^+$ (calcd for $C_{39}H_{41}N_5O_{14}Y^+$: 892.17), 914.112 $[M+Na]^+$ (calcd for $C_{39}H_{40}N_5O_{14}YNa^+$: 914.15), 930.848 $[M+K]^+$ (calcd for $C_{39}H_{40}N_5O_{14}YK^+$: 913.30), 952.077 $[M-H+Na+K]^+$ (calcd for $C_{39}H_{39}N_5O_{14}NaK^+$: 952.11), 990.048 $[M-2H+2Na+K]^+$ (calcd for $C_{39}H_{38}N_5O_{14}Na_2K^+$: 974.09). HR-MS ESI: m/z= 892.17407 $[M+H]^+$ (calcd for $C_{39}H_{41}N_5O_{14}Y^+$: 892.17030), 914.15265 $[M+Na]^+$ (calcd for $C_{39}H_{40}N_5O_{14}YNa^+$: 914.15225). UV-Vis (NaOH 0.1 M in water), λ_{max} (nm) (ε × 10^3 L.mol^{-1}.cm^{-1}): 491 (62.8). Fluorescence (NaOH 0.1 M in water), λ_{max} (nm) (Φ_F): 515 (0.856).

3.1.3. Fluorescein-DOTA ^{90}Y-1 (radiolabelled)

2,2',2''-(10-(1-carboxy-4-((3',6'-dihydroxy-3-oxo-3*H*-spiro[isobenzofuran-1,9'-xanthen]-5-yl)amino)-4-oxobutyl)-1,4,7,10-tetraazacyclododecane-1,4,7-triyl)triacetic acid ^{90}yttrium complex (**^{90}Y-1**). A solution of $[^{90}Y]$-YCl_3 (508.7 MBq, 1 mL) was purchased and used for radiolabelling studies. A solution of **1** (3.22 mg, 0.004 mmol) in 1 M ammonium acetate buffer (1 mL) was prepared. Several volumes of the solution of **1** (100 µL, 50 µL, 10 µL and 5 µL) were added to a constant volume of $[^{90}Y]$-YCl_3 (20 µL, 8-9 mBq); subsequent addition of ammonium acetate buffer (for experiments 3 and 4) allows to keep a pH value of 5.4:
Experiment 1: 100 µL of a **1** solution + 20 µL of $[^{90}Y]$-YCl_3 solution
Experiment 2: 50 µL of **1** solution + 20 µL of $[^{90}Y]$-YCl_3 solution
Experiment 3: 10 µL of **1** solution + 20 µL of $[^{90}Y]$-YCl_3 solution + 20 µL of $AcONH_4$ buffer
Experiment 4: 5 µL of **1** solution + 20 µL of $[^{90}Y]$-YCl_3 solution + 20 µL of $AcONH_4$ buffer
The mixtures were heated at 80°C for 2 hours. The reaction was monitored by RITLC. After cooling, the solutions were diluted with an appropriate volume of 0.1 M NaOH

solution (880 µL, 930 µL, 950 µL and 955 µL respectively) to obtain a total volume of 1 mL, subsequent emission measurements were then achieved.

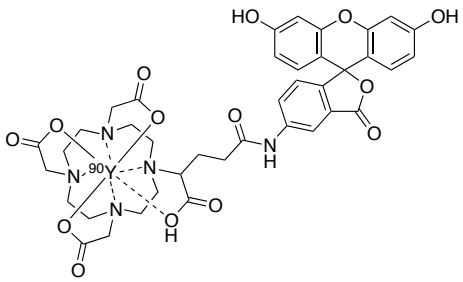

Radio-TLC (SiO_2, MeOH/$AcONH_4$ 50:50 vol.): Rf = 0.8
Experiment 1: 97.74 % radio-purity
Experiment 4: 96.04 % radio-purity

[^{90}Y]- Yttrium alone:

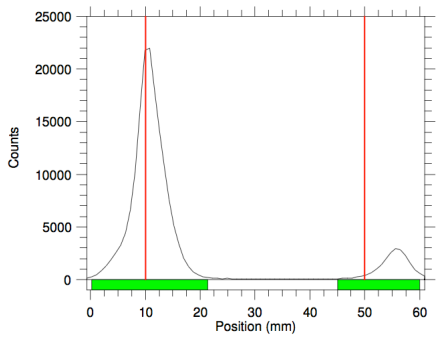

Experiment 1:

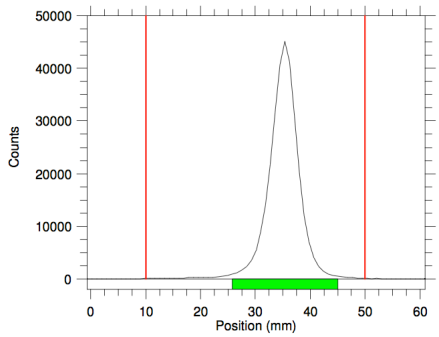

Experiment 4:

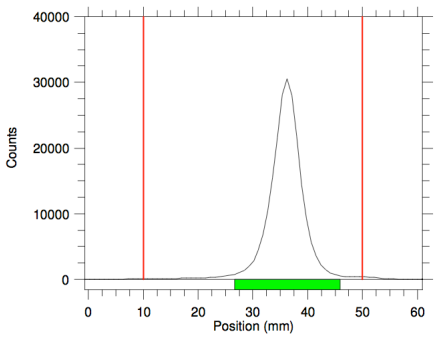

Fig. S8. Radio-TLC of commercial [^{90}Y]-YCl_3 solution; **^{90}Y-1**, experiment 1, 2 hours at 60°C and **^{90}Y-1**, experiment 4, 2 hours at 60°C (SiO_2, MeOH/$AcONH_4$ 50:50 vol.).

3.1.4. HPLC chromatograms and ^{1}H, MS, HRMS spectra of species 1 and ^{89}Y-1

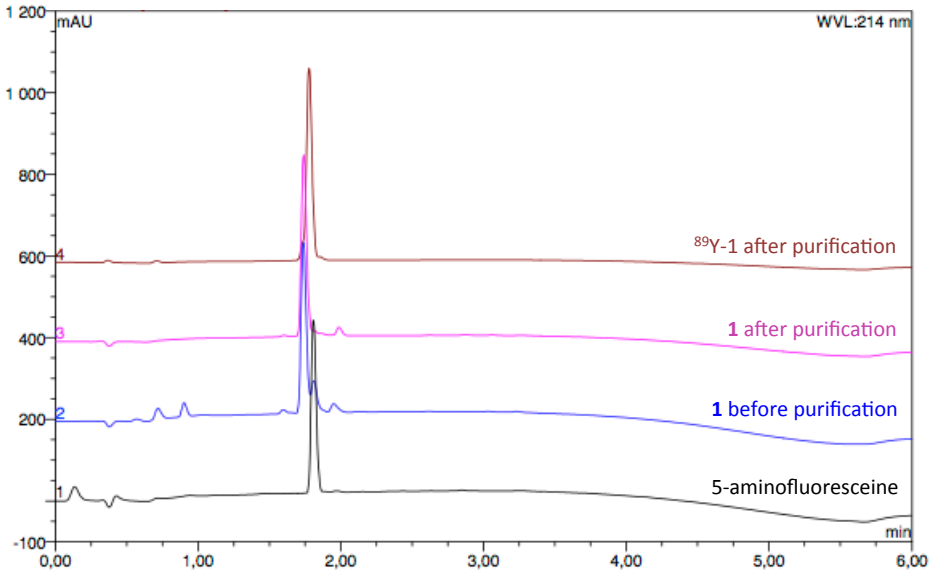

Fig. S9. HPLC chromatograms of 5-aminofluorescein, **1** before and after purification, and ^{89}Y-**1**.

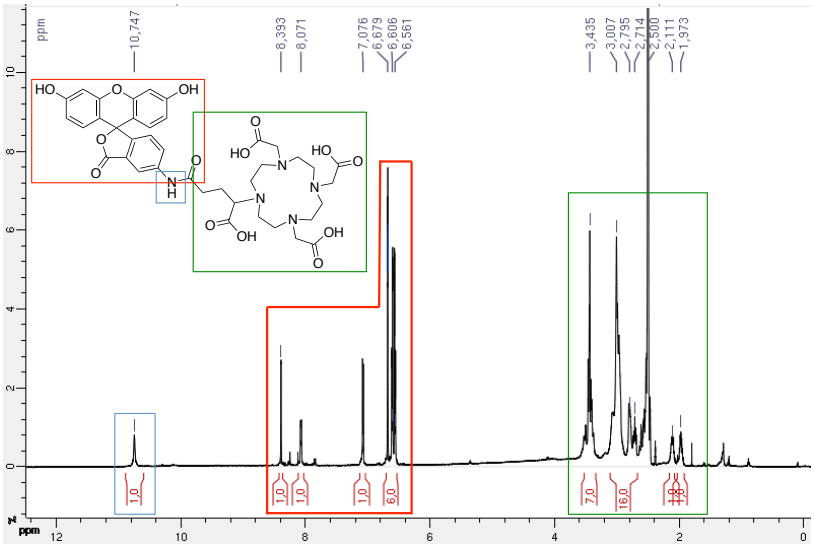

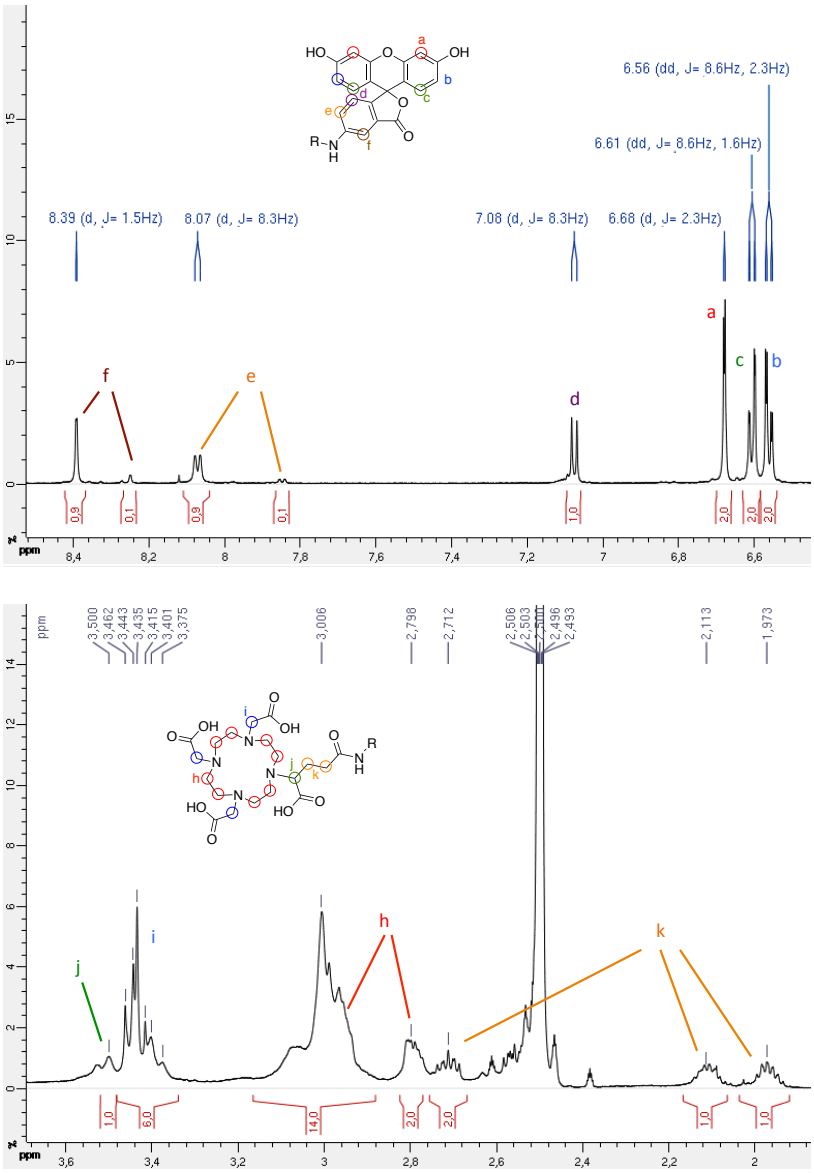

Fig. S10. ^{1}H NMR spectra of **1**, DMSO-d$_6$, 600 MHz, 420 K.

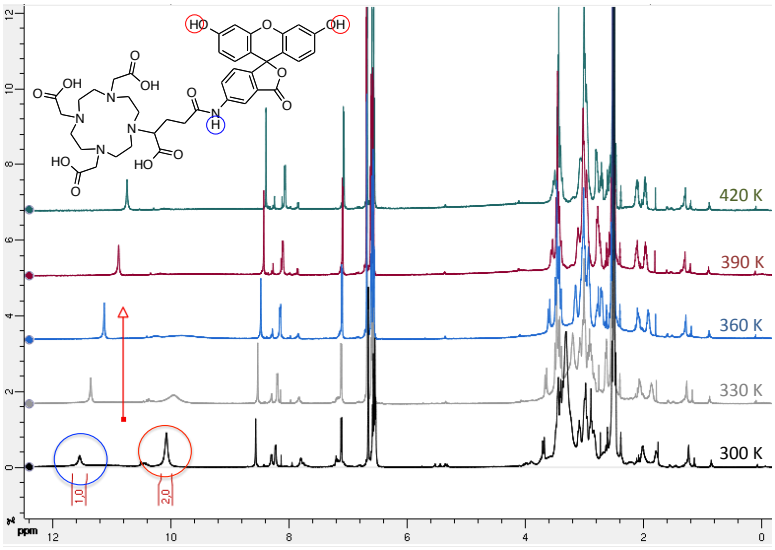

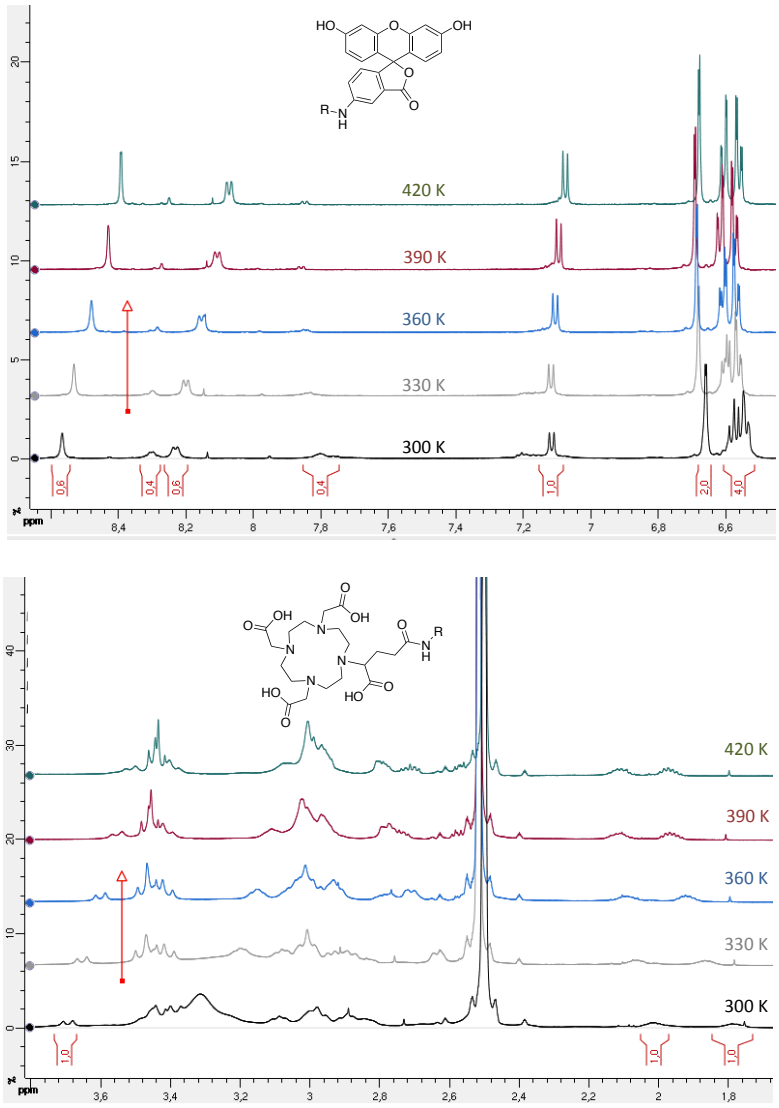

Fig. S11. ^{1}H NMR spectra of **1**, DMSO-d_6, 600 MHz, at various temperatures.

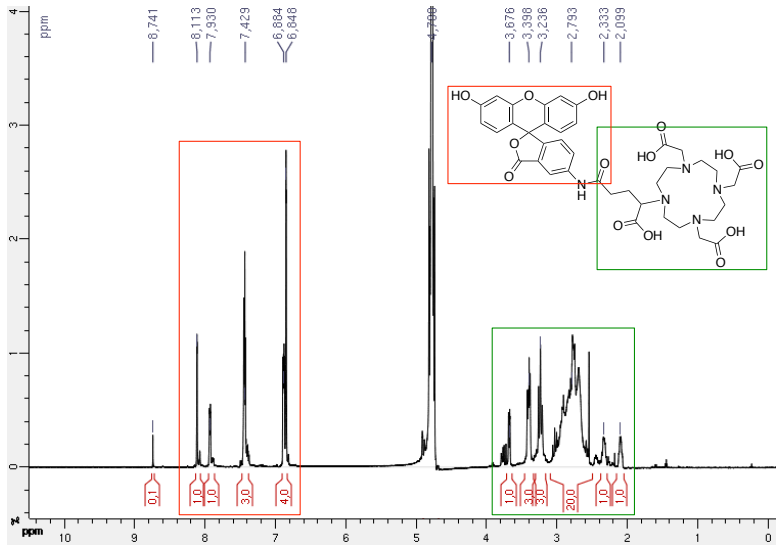

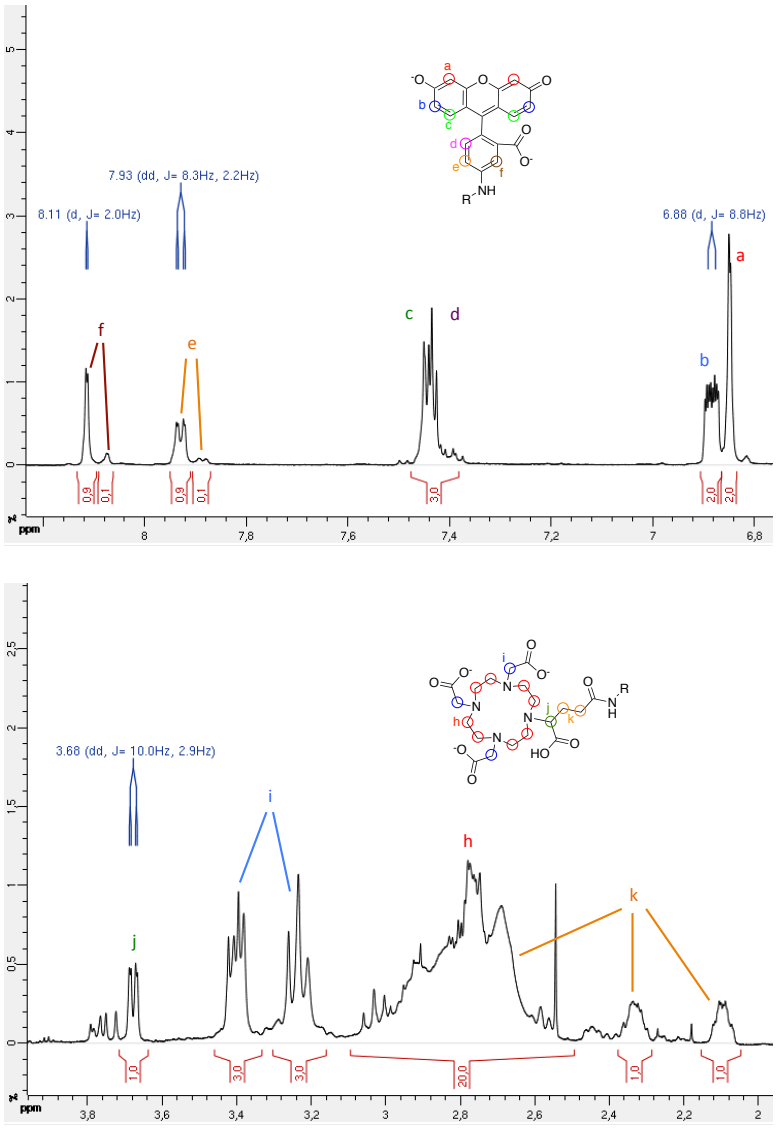

Fig. S12. ^{1}H NMR spectra of **1**, D_2O + NaOD, 600 MHz, 360 K.

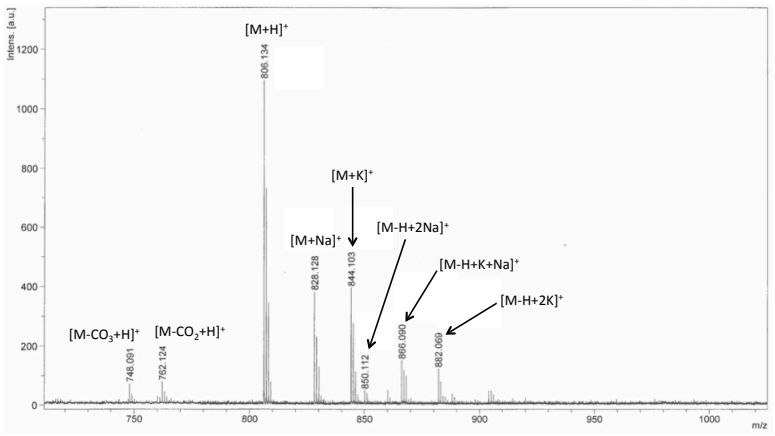

Fig. S13. MALDI-TOF MS spectrum of **1**.

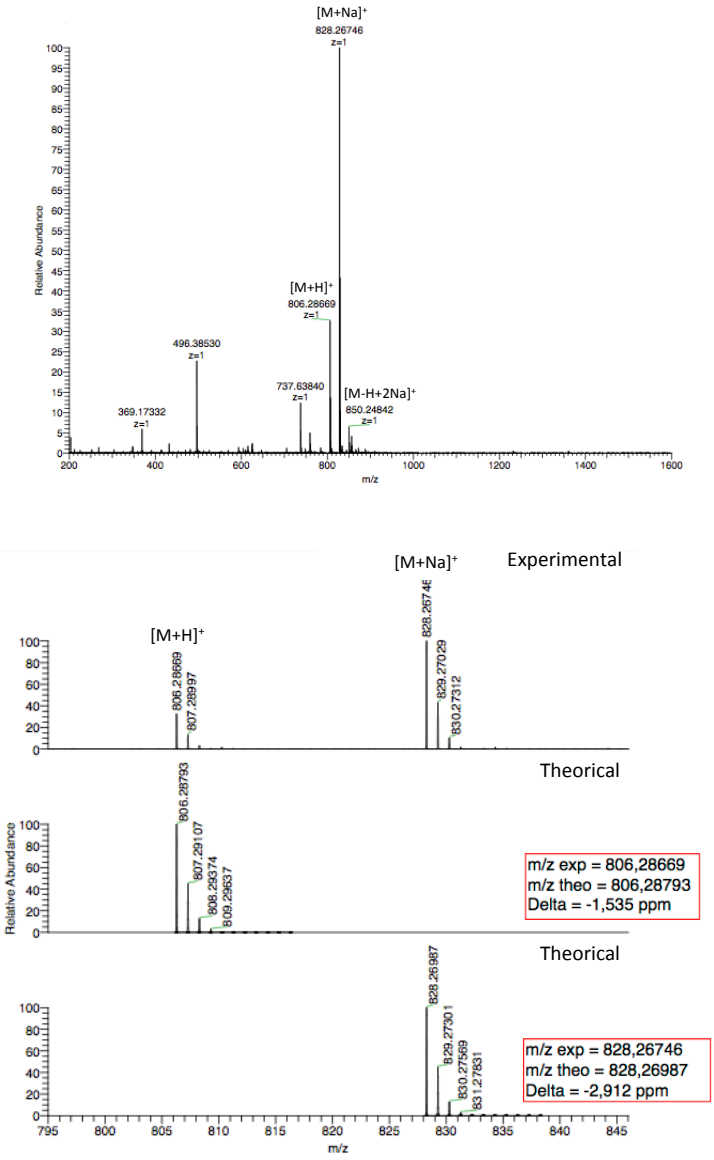

Fig. S14. High resolution MS spectra of **1**.

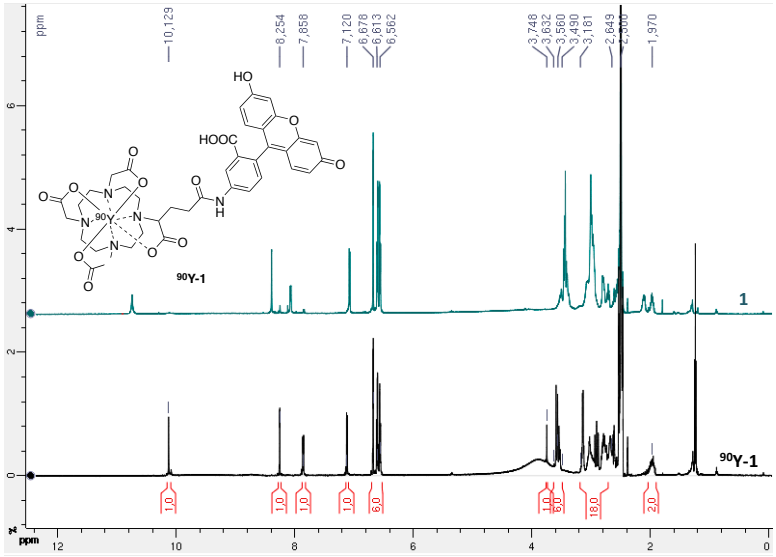

Fig. S15. ^{1}H NMR spectrum of **^{89}Y-1**, DMSO-d$_6$, 600 MHz, 390 K. Superimpose: ^{1}H NMR spectrum of **1**, DMSO-d$_6$, 600 MHz, 420 K.

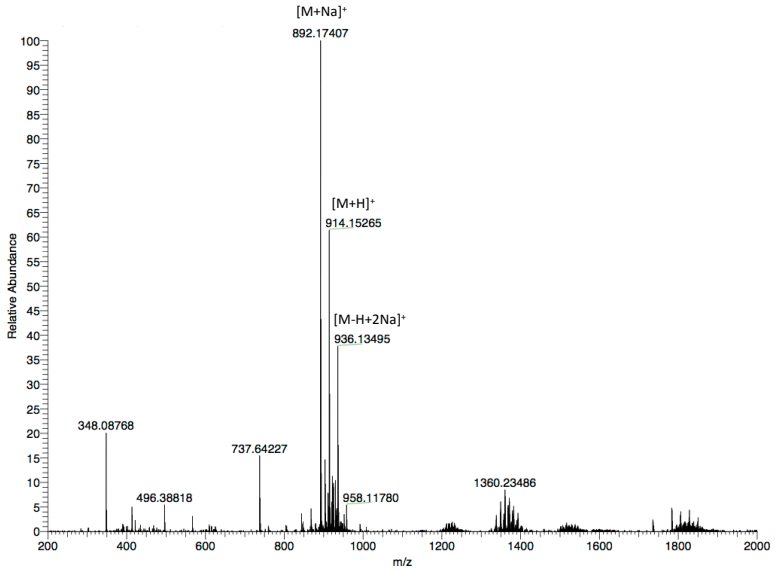

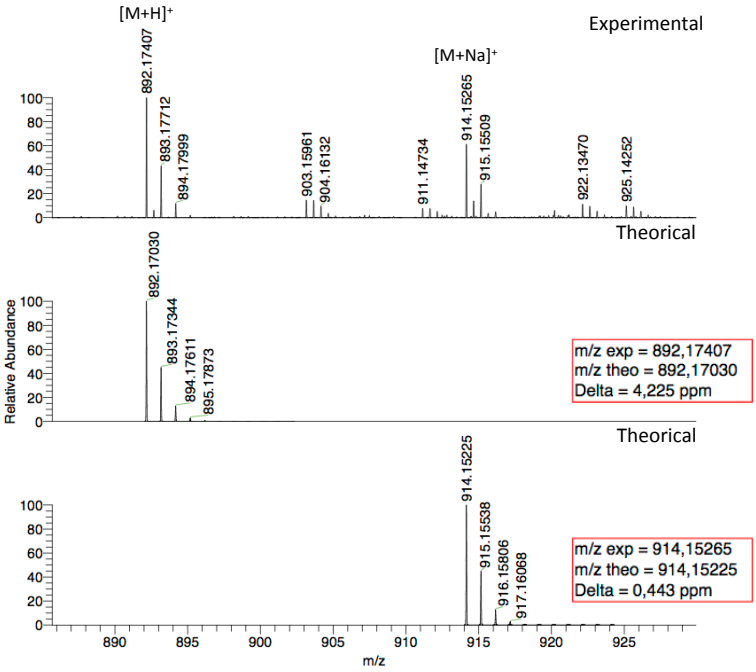

Fig. S16. HR-MS spectra of **^{89}Y-1**.

4. Additional References

All References related to Cerenkov Imaging are provided here; i.e. ca 70 papers since 2009.

1. Ackerman, N. L.; Graves, E. E., The potential for Cerenkov luminescence imaging of alpha-emitting radionuclides. Phys Med Biol 2012, 57 (3), 771-783.

2. Aweda, T. A.; Eskandari, V.; Kukis, D. L.; Boucher, D. L.; Marquez, B. V.; Beck, H. E.; Mitchell, G. S.; Cherry, S. R.; Meares, C. F., New Covalent Capture Probes for Imaging and Therapy, Based on a Combination of Binding Affinity and Disulfide Bond Formation. Bioconjugate Chem 2011, 22 (8), 1479-1483.

3. Beattie, B. J.; Thorek, D. L. J.; Schmidtlein, C. R.; Pentlow, K. S.; Humm, J. L.; Hielscher, A. H., Quantitative Modeling of Cerenkov Light Production Efficiency from Medical Radionuclides. Plos One 2012, 7 (2) e31402.

4. Boschi, F.; Pagliazzi, M.; Rossi, B.; Cecchini, M. P.; Gorgoni, G.; Salgarello, M.; Spinelli, A. E., Small-animal radionuclide luminescence imaging of thyroid and salivary glands with Tc-99m-pertechnetate. J Biomed Opt 2013, 18 (7).

5. Boschi, F.; Spinelli, A. E., Quantum dots excitation using pure beta minus radioisotopes emitting Cerenkov radiation. Rsc Adv 2012, 2 (29), 11049-11052.

6. Boschi, F.; Calderan, L.; D'Ambrosio, D.; Marengo, M.; Fenzi, A.; Calandrino, R.; Sbarbati, A.; Spinelli, A. E. In vivo 18F-FDG tumour uptake measurements in small animals using Cerenkov Radiation. Eur. J. Nucl. Med. Mol Imaging (2011 (38), 120-127.

7. Carpenter, C. M.; Sun, C.; Pratx, G.; Liu, H. G.; Cheng, Z.; Xing, L., Radioluminescent nanophosphors enable multiplexed small-animal imaging. Opt Express 2012, 20 (11), 11598-11604.

8. Cherry, S., Cerenkov luminescence imaging: a new tool for molecular imaging? J Nucl Med 2013, 54, 29-29.

9. Chin, P. T. K.; Welling, M. M.; Meskers, S. C. J.; Olmos, R. A. V.; Tanke, H.; van Leeuwen, F. W. B., Optical imaging as an expansion of nuclear medicine: Cerenkov-based luminescence vs fluorescence-based luminescence. Eur J Nucl Med Mol I 2013, 40 (8), 1283-1291.

10. Cho, J. S.; Taschereau, R.; Olma, S;; Liu, K.; Chen, Y.-C.; Shen, C. K.-F.; van Dam, R. M.; Chatziioannou, A. F.; Cerenkov Radiation imaging as a method for quantitative measurements of beta particles in a microfluidic chip. Phys. Med. Biol. 2009, 54, 6757-6771.

11. Darne, C.; Lu, Y. J.; Sevick-Muraca, E. M., Small animal fluorescence and bioluminescence tomography: a review of approaches, algorithms and technology update. Phys Med Biol 2014, 59 (1), R1-60.

12. Deh, K.; Fareedy, S.; Osborne, J., Calibration of a Cerenkov luminescence imaging probe for prostate cancer detection. J Nucl Med 2013, 54, 7-7.

13. Dooraghi, A. A.; Keng, P. Y.; Chen, S. P.; Javed, M. R.; Kim, C. J.; Chatziioannou, A. F.; van Dam, R. M., Optimization of microfluidic PET tracer synthesis with Cerenkov imaging. Analyst 2013, 138 (19), 5654-5664.

14. Dothager, R. S.; Goiffon, R. J.; Jackson, E.; Harpstrite, S.; Piwnica-Worms, D. Cerenkov Radiation Energy Transfer (CRET) imaging: a novel method for optical imaging of PET isotopes in biological systems.

15. Fahimian, B.; Ceballos, A.; Turkcan, S.; Kapp, D. S.; Pratx, G., Seeing the invisible: Direct visualization of therapeutic radiation beams using air scintillation. Med Phys 2014, 41 (1).

16. Fischer, G.; Seibold, U.; Schirrmacher, R.; Wangler, B.; Wangler, C., Zr-89, a Radiometal Nuclide with High Potential for Molecular Imaging with PET: Chemistry, Applications and Remaining Challenges. Molecules 2013, 18 (6), 6469-6490.

17. Holland, J. P.; Normand, G.; Ruggiero, A.; Lewis, J. S.; Grimm, J., Intraoperative Imaging of Positron Emission Tomographic Radiotracers Using Cerenkov Luminescence Emissions. Mol Imaging 2011, 10 (3), 177-186.

18. Hu, Z. H.; Chen, X. L.; Liang, J. M.; Qu, X. C.; Chen, D. F.; Yang, W. D.; Wang, J.; Cao, F.; Tian, J., Single photon emission computed tomography-guided Cerenkov luminescence tomography. J Appl Phys 2012, 112 (2) 024703.

19. Hu, Z. H.; Liang, J. M.; Yang, W. D.; Fan, W. W.; Li, C. Y.; Ma, X. W.; Chen, X. L.; Ma, X. P.; Li, X. S.; Qu, X. C.; Wang, J.; Cao, F.; Tian, J., Experimental Cerenkov luminescence tomography of the mouse model with SPECT imaging validation. Opt Express 2010, 18 (24), 24441-24450.

20. Hu, Z. H.; Ma, X. W.; Qu, X. C.; Yang, W. D.; Liang, J. M.; Wang, J.; Tian, J., Three-dimensional Noninvasive Monitoring Iodine-131 Uptake in the Thyroid Using a Modified Cerenkov Luminescence Tomography Approach. Plos One 2012, 7 (5) e37623.

21. Jeong, S. Y.; Hwang, M. H.; Kim, J. E.; Kang, S.; Park, J. C.; Yoo, J.; Ha, J. H.; Lee, S. W.; Ahn, B. C.; Lee, J., Combined Cerenkov luminescence and nuclear imaging of radioiodine in the thyroid gland and thyroid cancer cells expressing sodium iodide symporter: Initial feasibility study. Endocr J 2011, 58 (7), 575-583.

22. Kim, D. H.; Choe, Y. S.; Choi, J. Y.; Lee, K. H.; Kim, B. T., Binding of 2-[F-18]fluoro-CP-118,954 to mouse acetylcholinesterase: microPET and ex vivo Cerenkov luminescence imaging studies. Nucl Med Biol 2011, 38 (4), 541-547.

23. Klose, A.; System, Method and computer-accessible medium for performing attenuation-corrected multispectral luminescence tomography of Cerenkov and bioluminescent light sources. Intl Publication Number: WO 2011/137247 A2 (publication date: 03.11.2011); Intl Appln Number: PCT/US2011/034342; Intl Patent Classification: G06F 19/00 (2011.01) (New-York, Columbia University).

24. Kotagiri, N.; Niedzwiedzki, D. M.; Ohara, K.; Achilefu, S. Activatable probes based on distance-dependent luminescence associated with Cerenkov radiation. Angew. Chem. Int. Ed. 2013, 52, 7756-7760.

25. Kothapalli, S. R.; Liu, H. G.; Liao, J. C.; Cheng, Z.; Gambhir, S. S., Endoscopic imaging of Cerenkov luminescence. Biomed Opt Express 2012, 3 (6), 1215-1225.

26. Lewis, M. A.; Kodibagkar, V. D.; Oz, O. K.; Mason, R. P., On the potential for molecular imaging with Cerenkov luminescence. Opt Lett 2010, 35 (23), 3889-3891.

27. Li, C. Q.; Mitchell, G. S.; Cherry, S. R., Cerenkov luminescence tomography for small-animal imaging. Opt Lett 2010, 35 (7), 1109-1111.

28. Liu, H. G.; Carpenter, C. M.; Jiang, H.; Pratx, G.; Sun, C.; Buchin, M. P.; Gambhir, S. S.; Xing, L.; Cheng, Z., Intraoperative Imaging of Tumors Using Cerenkov Luminescence Endoscopy: A Feasibility Experimental Study. J Nucl Med 2012, 53 (10), 1579-1584.

29. Liu, H. G.; Carpenter, C. M.; Jiang, H.; Pratx, G.; Sun, C.; Buchin, M. P.; Gambhir, S. S.; Xing, L.; Cheng, Z., Fiber-based system for imaging tumor margins with Cerenkov Luminescence. Abstr Pap Am Chem S 2012, 243.

30. Liu, H.; Ren, G.; Miao, Z.; Zhang, X;; Tang, X.; Han, P.; Gambhir, S. S.; Cheng, Z. Molecular optical imaging with radioactive probes. PLoS one, 2010, 5 (3), e9470.

31. Lucignani, G. Cerenkov radioactive optical imaging: a promising new strategy

32. Ma, X. W.; Kang, F.; Xu, F.; Feng, A. L.; Zhao, Y.; Lu, T. J.; Yang, W. D.; Wang, Z.; Lin, M.; Wang, J., Enhancement of Cerenkov Luminescence Imaging by Dual Excitation of Er3+, Yb3+-Doped Rare-Earth Microparticles. Plos One 2013, 8 (10) e77926.

33. Mitchell, G. S.; Gill, R. K.; Boucher, D. L.; Li, C. Q.; Cherry, S. R., In vivo Cerenkov luminescence imaging: a new tool for molecular imaging. Philos T R Soc A 2011, 369 (1955), 4605-4619.

34. Mitchell, G. S.; Gill, R. K.; Cherry, S. R. Comments on 'Cerenkov radiation allows in vivo optical imaging of positron emitting radiotracers' Phys. Med. Biol. 2010, 55, L43-L44.

35. Natarajan, A.; Habte, F.; Liu, H. G.; Sathirachinda, A.; Hu, X.; Cheng, Z.; Nagamine, C. M.; Gambhir, S. S., Evaluation of Zr-89-rituximab Tracer by Cerenkov Luminescence Imaging and Correlation with PET in a Humanized Transgenic Mouse Model to Image NHL. Mol Imaging Biol 2013, 15 (4), 468-475.

36. Park, J. C.; An, G. I.; Park, S. I.; Oh, J.; Kim, H. J.; Ha, Y. S.; Wang, E. K.; Kim, K. M.; Kim, J. Y.; Lee, J.; Welch, M. J.; Yoo, J., Luminescence imaging using radionuclides: a potential application in molecular imaging. Nucl Med Biol 2011, 38 (3), 321-329.

37. Qin, C.; Ma, X.; Tian, J., Translational Research of Optical Molecular Imaging for Personalized Medicine. Curr Mol Med 2013, 13 (10), 1579-1590.

38. Qin, C. H.; Zhong, J. H.; Hu, Z. H.; Yang, X.; Tian, J., Recent Advances in Cerenkov Luminescence and Tomography Imaging. Ieee J Sel Top Quant 2012, 18 (3), 1084-1093.

39. Qin, C. X.; Cheng, K.; Chen, K.; Hu, X.; Liu, Y.; Lan, X. L.; Zhang, Y. X.; Liu, H. G.; Xu, Y. D.; Bu, L. H.; Su, X. H.; Zhu, X. H.; Meng, S. X.; Cheng, Z., Tyrosinase as a multifunctional reporter gene for Photoacoustic/MRI/PET triple modality molecular imaging. Sci Rep-Uk 2013, 3.

40. Ran, C. Z.; Zhang, Z. D.; Hooker, J.; Moore, A., In Vivo Photoactivation Without "Light": Use of Cherenkov Radiation to Overcome the Penetration Limit of Light. Mol Imaging Biol 2012, 14 (2), 156-162.

41. Robertson, R.; Germanos, M. S.; Li, C.; Mitchell, G. S.; Cherry, S. R.; Silva, M. D., Optical imaging of Cerenkov light generation from positron-emitting radiotracers. Phys Med Biol 2009, 54 (16), N355-N365.

42. Robertson, R.; Germanos, M. S.; Manfredi, M. G.; Smith, P. G.; Silva, M. D., Multimodal Imaging with F-18-FDG PET and Cerenkov Luminescence Imaging After MLN4924 Treatment in a Human Lymphoma Xenograft Model. J Nucl Med 2011, 52 (11), 1764-1769.

43. Ruggiero, A.; Holland, J. P.; Lewis, J. S.; Grimm, J., Cerenkov Luminescence Imaging of Medical Isotopes. J Nucl Med 2010, 51 (7), 1123-1130.

44. Silva, I.; Pang, G. Electronic portal Imaging using Cerenkov radiation. Radiotherapy and Oncology, 2007, 2, S93.

45. Spinelli, A. E.; Boschi, F., Unsupervised analysis of small animal dynamic Cerenkov luminescence imaging. J Biomed Opt 2011, 16 (12) 120507-1-3.

46. Spinelli, A. E.; Boschi, F., Optimizing in vivo small animal Cerenkov luminescence imaging (vol 17, 040506, 2012). J Biomed Opt 2012, 17 (5).

47. Spinelli, A. E.; Boschi, F., Optimizing in vivo small animal Cerenkov luminescence imaging. J Biomed Opt 2012, 17 (4).

48. Spinelli, A. E.; Ferdeghini, M.; Cavedon, C.; Zivelonghi, E.; Calandrino, R.; Fenzi, A.; Sbarbati, A.; Boschi, F., First human Cerenkography. J Biomed Opt 2013, 18 (2).

49. Spinelli, A. E.; Kuo, C.; Rice, B. W.; Calandrino, R.; Marzola, P.; Sbarbati, A.; Boschi, F., Multispectral Cerenkov luminescence tomography for small animal optical imaging. Opt Express 2011, 19 (13), 12605-12618.

50. Spinelli, A. E.; Lo Meo, S.; Calandrino, R.; Sbarbati, A.; Boschi, F., Optical imaging of Tc-99m-based tracers: in vitro and in vivo results. J Biomed Opt 2011, 16 (11).

51. Spinelli, A. E.; Marengo, M.; Calandrino, R.; Sbarbati, A.; Boschi, F., Optical imaging of radioisotopes: a novel multimodal approach to molecular imaging. Q J Nucl Med Mol Im 2012, 56 (3), 280-290.

52. Spinelli, A. E.; D'Ambrosio, D.; Calderan, L.; Marengo, M.; Sbarbati, A.; Boschi, F. Cerenkov Radaition allows in vivo optical imaging of positron emitting radiotracers. Phys Med Biol, 2010, 55 (2), 483-495.

53. Spinelli, A. E.; D'Ambrosio, D;; Calderan, L.; Marengo, M.; Sbarbati, A;; Boschi, F. Reply to 'Comments on "Cerenkov radiation allows in vivo optical imaging of positron emitting radiotracers'" Phys Med Biol, 2010, 55, L45-L49.

54. Sun, C.; Pratx, G.; Carpenter, C. M.; Liu, H. G.; Cheng, Z.; Gambhir, S. S.; Xing, L., Synthesis and Radioluminescence of PEGylated Eu3+-doped Nanophosphors as Bioimaging Probes. Adv Mater 2011, 23 (24), H195-H199.

55. Thorek, D. L. J.; Holland, J.; Normand, G.; Ruggiero, A.; Lewis, J. S.; Grimm, J., Cerenkov luminescence imaging for the use of PET tracers in the intraoperative setting. J Labelled Compd Rad 2011, 54, S22-S22.

56. Thorek, D. L. J.; Ogirala, A.; Beattie, B. J.; Grimm, J., Quantitative imaging of disease signatures through radioactive decay signal conversion. Nat Med 2013, 19 (10), 1345-1350.

57. Thorek, D. L. J.; Riedl, C. C.; Grimm, J., Clinical Cerenkov Luminescence Imaging of F-18-FDG. J Nucl Med 2014, 55 (1), 95-98.

58. Wang, Y. C.; Liu, Y. J.; Luehmann, H.; Xia, X. H.; Wan, D. H.; Cutler, C.; Xia, Y. N., Radioluminescent Gold Nanocages with Controlled Radioactivity for Real-Time in Vivo Imaging. Nano Lett 2013, 13 (2), 581-585.

59. Xu, Y. D.; Chang, E.; Liu, H. G.; Jiang, H.; Gambhir, S. S.; Cheng, Z., Proof-of-Concept Study of Monitoring Cancer Drug Therapy with Cerenkov Luminescence Imaging. J Nucl Med 2012, 53 (2), 312-317.

60. Xu, Y. D.; Liu, H. G.; Cheng, Z., Harnessing the Power of Radionuclides for Optical Imaging: Cerenkov Luminescence Imaging. J Nucl Med 2011, 52 (12), 2009-2018.

61. Yang, W. D.; Qin, W. W.; Hu, Z. H.; Suo, Y. Y.; Zhao, R.; Ma, X. W.; Ma, W. H.; Wang, T.; Liang, J. M.; Tian, J.; Wang, J., Comparison of Cerenkov Luminescence Imaging (CLI) and gamma camera imaging for visualization of let-7 expression in lung adenocarcinoma A549 Cells. Nucl Med Biol 2012, 39 (7), 948-953.

62. Zhang, J. G.; Liu, H. F., Functional imaging and endoscopy. World J Gastroentero 2011, 17 (38), 4277-4282.

63. Zhang, R. X.; Gladstone, D. J.; Jarvis, L. A.; Strawbridge, R. R.; Hoopes, P. J.; Friedman, O. D.; Glaser, A. K.; Pogue, B. W., Real-time in vivo Cherenkoscopy imaging during external beam radiation therapy. J Biomed Opt 2013, 18 (11).

64. Zhang, X. L.; Kuo, C.; Moore, A.; Ran, C. Z., In Vivo Optical Imaging of Interscapular Brown Adipose Tissue with F-18-FDG via Cerenkov Luminescence Imaging. Plos One 2013, 8 (4).

65. Zhang, X. L.; Ran, C. Z., Dual Functional Small Molecule Probes as Fluorophore and Ligand for Misfolding Proteins. Curr Org Chem 2013, 17 (6), 580-593.

66. Zhong, J. H.; Qin, C. H.; Yang, X.; Chen, Z.; Yang, X.; Tian, J., Fast-Specific Tomography Imaging Cerenkov Emission. Mol Imaging Biol 2012, 14 (3), 286-292.

67. Zhong, J. H.; Tian, J.; Liu, H. X.; Qin, C. H.; Yang, X.; Ma, X. B., Tomographic reconstruction of Cerenkov photons in tissues through approximate message-passing. Proc Spie 2012, 8314.

68. Zhong, J. H.; Tian, J.; Yang, X.; Qin, C. H., Whole-Body Cerenkov Luminescence Tomography with the Finite Element SP3 Method. Ann Biomed Eng 2011, 39 (6), 1728-1735.